Published in final edited form as:
J Neurosurg Spine. 2013 August ; 19(2): 248–255. doi:10.3171/2013.4.SPINE12961.

Reliability in the Location of Hindlimb Motor Representations in Fischer-344 Rats

Shawn B. Frost, Ph.D.[1,2], **Maria Iliakova, M.S.**[3], **Caleb Dunham, B.S.**[1], **Scott Barbay, Ph.D.**[1], **Paul Arnold, MD**[3,4], and **Randolph J. Nudo, Ph.D.**[1,2]

[1]Landon Center On Aging, University of Kansas Medical Center, Kansas City, KS, USA

[2]Dept. of Molecular & Integrative Physiology, University of Kansas Medical Center, Kansas City, KS, USA

[3]School of Medicine, University of Kansas Medical Center, Kansas City, KS, USA

[4]Department of Neurosurgery, University of Kansas Medical Center, Kansas City, KS, USA

Abstract

Object—The purpose of the present study was to determine the feasibility of using a common laboratory rat strain for locating cortical motor representations of the hindlimb reliably.

Methods—Intracortical Microstimulation (ICMS) techniques were used to derive detailed maps of the hindlimb motor representations in six adult Fischer-344 rats.

Results—The organization of the hindlimb movement representation, while variable across individuals in topographic detail, displayed several commonalities. The hindlimb representation was positioned posterior to the forelimb motor representation and postero-lateral to the motor trunk representation. The areal extent of the hindlimb representation across the cortical surface averaged 2.00 +/− 0.50 mm^2. Superimposing individual maps revealed an overlapping area measuring 0.35 mm^2, indicating that the location of the hindlimb representation can be predicted reliably based on stereotactic coordinates. Across the sample of rats, the hindlimb representation was found 1.25–3.75 mm posterior to Bregma, with an average center location ~ 2.6 mm posterior to Bregma. Likewise, the hindlimb representation was found 1–3.25 mm lateral to the midline, with an average center location ~ 2 mm lateral to midline.

Conclusions—The location of the cortical hindlimb motor representation in Fischer-344 rats can be reliably located based on its stereotactic position posterior to Bregma and lateral to the longitudinal skull suture at midline. The ability to accurately predict the cortical localization of functional hindlimb territories in a rodent model is important, as such animal models are being used increasingly in the development of brain-computer interfaces for restoration of function after spinal cord injury.

Corresponding Author: Shawn B. Frost, Ph.D., Dept. of Molecular & Integrative Physiology, University of Kansas Medical Center, Mail Stop: 4016, Kansas City, KS, USA, 913-588-7394, FAX: 913-945-6827, sfrost@kumc.edu.

No portion of this work has been presented elsewhere.

Author contributions to the study and manuscript preparation include the following. Conception and design: Frost, Nudo. Acquisition of data: Frost, Dunham, Barbay. Analysis and interpretation of data: Frost, Iliakova, Dunham, Nudo. Drafting the article: Frost, Nudo, Arnold. Critically revising the article: Frost, Iliakova, Arnold, Nudo. Reviewed submitted version of manuscript: Frost, Nudo, Iliakova, Dunham, Barbay, Arnold. Approved the final version of the manuscript on behalf of all authors: Frost, Nudo. Statistical analysis: Frost. Study supervision: Nudo.

DISCLOSURE

The authors report no conflict of interest concerning the materials or methods used in this study or findings specified in this paper.

Keywords

Motor Cortex; Hindlimb; Fischer-344; Intracortical Microstimulation

After injury to the spinal cord, while the descending motor pathways, such as the corticospinal tract, are often damaged, the motor cortex remains intact. Recently, neuroprosthetic approaches to restore function have taken advantage of this fact by developing brain-computer interfaces that discriminate neural activity in the intact motor cortex to use as control signals to activate external devices[9] or the contraction of individual skeletal muscles.[6] As human applications are still in very early stages, animal models continue to play a critical role in the development of future smart prosthetic technologies. Any reliable neuroprosthetic device will require technological development in an animal model before it can be tested in spinal cord injury patients. The purpose of the present study was to determine the feasibility of using a common laboratory rat strain for locating cortical motor representations reliably, even after a spinal cord injury. Specifically, we focused on the reliability of the hindlimb motor representation in rats with respect to stereotactic coordinates. The ability to locate the hindlimb motor area will allow for the potential use of neural activity in intact cortex of spinal cord injured rats for the development of a neuroprosthetic device.

In a typical brain-computer interface, microelectrodes used for discriminating individual action potentials as control signals are placed within the part of the motor cortex innervating motor neurons in the spinal cord below the level of the lesion. In an intact nervous system, identification is straight-forward, since stimulation of the cortex can be used to determine cortical locations that result in movement of the appropriate skeletal musculature. However, since corticospinal fibers are often compromised in spinal cord injury, such identification is not possible. If it can be demonstrated that the location of a specific cortical motor representation is sufficiently reliable, then stereotactic coordinates could be used for identification, even after spinal cord injury. These findings may be useful in translating these devices into human use. For example, animal models might be used for the development of robust microelectrode technology, or optimizing control algorithms. There currently is no cure for human spinal cord injury, and past attempts involving multicenter drug trials have been disappointing. Until adequate pharmacologic or cellular therapies are developed, prosthetic devices that bypass the injured spinal cord segment may be useful in promoting muscle activity and restoration of function.

To this end, we used intracortical microstimulation techniques to examine the location and organization of the hindlimb movement representation in a small sample of normal, neurologically intact, laboratory rats. Rats are an appropriate species for these experiments as true motor cortex is evident with a reversed motor representation (M1) rostral to the somatosensory representation (see Nudo and Frost, 2006 for review),[18] and rats have descending cortical projections to the spinal cord that are involved in voluntary control of movement; similar to that seen in primates.[20] Furthermore, comparative analyses of motor movements in rats and primates show homology of many motor patterns across species.[4] The results presented here demonstrate that while individual rats vary widely with respect to specific movement representations contained within the map, the extent and location of the hindlimb area is highly predictable, suggesting that this strain of laboratory rat is a suitable model for the further development of neuroprosthetic approaches after spinal cord injury.

METHODS

Subjects

Six, adult, Fischer-344 inbred rats (Harlan Laboratories, Indianapolis, IN) were selected for this study. This strain of rat has been increasingly used as a model subject in experiments examining spinal cord injury resulting in impairment of hindlimb movements.[3,10,15,16,23,26,28] Body weights ranged from 304g to 420g (mean= 353 +/− 54g) and ages were 3.2 to 9 months old.

This study was performed in accordance with all standards detailed in the *Guide for the Care and Use of Laboratory Animals* (Institute for Laboratory Animal Research, National Research Council, Washington, DC: National Academy Press, 1996). The protocol was approved by the University of Kansas Medical Center Institutional Animal Care and Use Committee.

Surgical and electrophysiological procedures

Standard techniques for mapping the representations of movements in motor cortex were used. Details of the electrophysiological procedures have been reported in previous publications.[13,19,21] Briefly, all surgical procedures were conducted under aseptic conditions. After an initial anesthetic state was reached using isoflurane anesthesia (to prepare the rat for injection), isoflurane was withdrawn and an intraperitoneal injection of ketamine hydrochloride (100mg/kg) and xylazine (5mg/kg) anesthesia was administered. . The rats were placed in a Kopf small-animal stereotaxic instrument (David Kopf Instruments ®, Tujunga, CA) and the incisor bar was adjusted until the heights of lambda and bregma skull points were equal (flat skull position). Using a number 11 scalpel blade the cisterna magna was punctured at the base of the skull to reduce edema during mapping. Next, the scalp was incised. Then a craniectomy was performed over the motor cortex by thinning the skull over primary motor cortex using a small Dremel drill bit and peeling off the thinned bone flap using fine microforceps. The general location of the craniectomy was based on previous motor mapping studies in the rat and was intentionally larger than the anticipated location of the hindlimb motor cortex.[13] The dura over the cranial opening was incised with small vanna scissors and removed. Then the opening was filled with warm, medical grade sterile silicone oil (50% Medical Silicone Fluid 12,500, 50% MDM Silicone Fluid 1000, Applied Silicone Corporation, Santa Paula, CA).

Throughout the experimental procedure, core temperature and vital signs were monitored. Core temperature was measured using a rectal probe, and temperature was maintained within the normal physiological range (~ 37.5^{o}C) using a feedback-controlled heating pad during the entire procedure. Care was taken to maintain a relatively stable anesthetic state. The anesthetic level was assessed by careful periodic monitoring of the respiratory and heart rate, as well as degree of muscle tone. Intracortical microstimulation (ICMS) mapping procedures were conducted only during periods of stable ketamine anesthesia and were halted during occasional periods of shallow (excessive muscle tone in the limbs and rapid heart rate) or deeper anesthesia (marked by unusually high ICMS thresholds). A single bolus of ketamine (10mg i.m.) was administered when an increased heart and respiration rate, or increased muscle tone warranted a need for a deeper anesthetic state.

A magnified digital photograph of the cortical surface was obtained through a surgical microscope and displayed on a computer monitor. A 250 μm grid pattern was placed over the image to indicate intended sites for microelectrode penetration. The stimulating microelectrode consisted of a platinum wire insulated into a glass micropipette filled with 3.5 M NaCl solution. A standard pipette puller (Sutter Instrument Co., USA) was used to

create a tapered tip with a diameter of 15–20 μm. The tip was beveled at a sharp angle using a micropipette beveler (K.T. Brown Type, Sutter Instrument Co., USA), allowing the thin micropipette to easily penetrate through the pia. Microelectrode impedance ranged from 750 kΩ-1 MΩ). Microelectrodes were advanced perpendicular to the cortical surface and advanced to a depth of ~1700 μm (the approximate location of layer 5 in this species), using a hydraulic microdrive (David Kopf Instruments ®, Tujunga, CA). The stimulus consisted of thirteen 200μs cathodal pulses delivered at 350 Hz repeated at 1/sec from an electrically isolated, charge-balanced (capacitively coupled) stimulation circuit. The electrodes were introduced at interpenetration distances of 250μm using the fine grid pattern sited with reference to the surface vasculature. At each penetration site, conventional ICMS techniques were used to define evoked movements. The current waveform was monitored by observing the voltage drop across a 10 kΩ resistor in series with the stimulation circuit.

Movement fields were defined by movements evoked by ICMS at near-threshold current levels (maximum current 60 μA). For forelimb and hindlimb movements, these movements were evoked almost exclusively in the contralateral side of the body. For trunk movements, laterality typically was not discernible. At each site, current was gradually increased from zero until a movement response could be defined reliably by visual inspection. After the evoked movement was defined, the current was decreased until the movement ceased, and then gradually increased again to determine the current intensity needed to evoke the movement in at least 50% of the train bursts. This current intensity was defined as the threshold current level. At each site, two observers independently determined the threshold movement and threshold current. A movement was recorded only when motion about a joint was observed; i.e., muscle twitches were not considered responses until an anti-gravity type response was seen. The hindlimb was manipulated only when it was necessary to stablilize the leg in order to distinquish between ankle and toe movements. If a response was not evoked at 60 μA, stimulation was halted and the site was designated as nonresponsive.

The extent of the hindlimb representation across the cortical surface was explored as completely as possible. Penetrations were made at each intersection on the 250 μm grid pattern (avoiding blood vessels) until the hindlimb area was circumscribed by sites evoking either forelimb movements, trunk movements or no visible response. Nonresponsive sites were verified later in a second attempt to evoke movement in the same mapping procedure. Further details of these procedures and discussion of possible sources of variation in ICMS-derived motor maps are found elsewhere.[7,19,21]

Map construction and areal measurements

From the neurophysiologic data, representational map boundaries were determined to outline different cortical efferent zones. Each zone contained microelectrode penetration sites at which stimulation evoked a specific movement. The procedure was as follows: The X-Y coordinates of each penetration site were determined from their locations indicated on the magnified digital photograph of the surface vasculature. Each response-type was assigned a unique color. Representational maps of response zones were generated by a custom computer algorithm that used the x-y location of electrode penetrations to establish unbiased borders midway between adjacent sites with different response representations (different colors). The hindlimb representation was defined as the cortical region within which ICMS evoked visible movements of the hindlimb at near-threshold current levels. These movements included flexion, extension, and adduction of the toe, ankle, knee or leg (hip). The colored representational maps were analyzed using an image analysis program (Scion Image, v1.63) that measured spatial parameters of regions representing different movement categories, coded by different colors.[19]

RESULTS

Functional organization of the hindlimb area

Using ICMS parameters described in Methods, hindlimb movements were evoked in each of the six rats at relatively low current levels (<70 μA). All evoked movements were observed in the contralateral musculature, except where noted. As the entire extent of the hindlimb representation was explored in each of the six rats, maps of evoked hindlimb movements were reconstructed from the movements evoked at individual sites. These hindlimb movement maps revealed an internal topography that appeared as a complex mosaic pattern (Figure 1), similar to forelimb representations described in previous studies.[13,19] The topography of the mosaical movement maps was variable across individuals, though several commonalities were evident. In all six rats, the hindlimb representation was positioned posterior to the forelimb representation and postero-lateral to the trunk representation. Also, the knee and toe representations tended to be positioned lateral or postero-lateral to the leg/hip and ankle representations (Figure 1–2).

At the minimum current levels required to evoke movement, nearly all (98.4%) hindlimb movements were observed in the contralateral hindlimb (179/182). However, at three sites, movements were evoked at the ipsilateral knee joint (2 extensions, 1 flexion).

The areal extents of hindlimb movement representations in the individual rats are shown in Table 1. The size of the hindlimb representation ranged from 1.23 to 2.51 mm^2 and averaged 2.00 +/− 0.50 mm^2. The leg/hip representation ranged from 0.87 to 1.81 mm^2 with an average of 1.24 +/− 0.39 mm^2. The knee representation was observed in 4 of 6 rats, with a range of 0 to 0.37 mm^2, averaging 0.18+/− 0.15mm^2. The ankle representation ranged from 0.07 to 0.75 mm^2, averaging 0.32 +/− 0.25 mm^2. The toe representation was observed in 5 of 6 rats, with a range of 0 to 0.68 mm^2 and averaging 0.26+/− 0.30mm^2.

ICMS-evoked ankle and toe movements were exclusively flexions. That is, no ankle or toe extensions were observed. The majority (84.6%) of ICMS-evoked knee movements were also flexions (11/13), with the exception of two sites at which knee extension movements were evoked. Most (89.6%) leg/hip movements were flexions (103/115) while 10.4 % were adductions (12/115).

A linear regression analysis of the variation in the size of each rat and the size of the total hindlimb area showed that there was no significant relationship between weight (g) and hindlimb area (mm^2) (R^2= 0.112; P= .516)

Movement Thresholds

Minimum currents required to evoke movements (movement thresholds) are shown in Table 2. The average of mean thresholds for all hindlimb movements across rats was 33.8 +/− 4.8 μA. An analysis of variance found no statistical difference between hindlimb movement thresholds or between hindlimb and movement thresholds of the forelimb. Mean minimum thresholds for movement of the forelimb was 35.7 +/− 5.4 μA (see table 2).

Maps of relative currents required to evoke hindlimb movements in individual rats are shown graphically in Figure 3, with red areas indicating regions requiring the lowest current levels and blue areas indicating regions requiring the highest current levels. The distribution of minimum required currents was highly variable across rats. However, though not quantitatively analyzed, there appeared to be a trend towards lower movement thresholds (red) located in the anterior portion of the map in each rat.

Reliability in Location of the Hindlimb Representation

To determine the reliability of the stereotactic position of the hindlimb representation (relative to Bregma), the borders generated in each rat were superimposed on a single coordinate plane (Figure 4, Left). While some variability in exact position can be seen, the location of hindlimb maps was remarkably similar. It was evident that at least a small cortical region contained part of the hindlimb representation in each of the six rats. The hindlimb movement representation ranged from 1.25–3.75 mm posterior to Bregma, with an average center location ~ 2.5 mm posterior to Bregma. Likewise, the hindlimb movement representation was found 1.00–3.25 mm lateral to Bregma (midline), with an average center location ~ 2 mm lateral to Bregma.

To further quantify the degree of overlap, the six maps were stacked in a commercial graphics program (Canvas, ACD Systems). Each map was filled with light grey of the same density, and then the opacity of each map was set to 16.7% (1/6). This resulted in a composite map with the zone of greatest overlap (most rats) showing the darkest grey fill. Then, the borders of the grey regions were smoothed to create a final hindlimb probability map (Figure 4, Right). The highest probability area where hindlimb movements were observed in all six rats was approximately 0.35 mm^2. The center of the high probability zone was at 2.00 mm posterior to Bregma and 2.64 mm lateral to Bregma (midline).

DISCUSSION

The motor map of the hindlimb in rat

The motor area of the neocortex of the rat has been identified as the area in which movements are evoked by the lowest intensity of electrical stimulation.[5] The organization of movement representations within motor cortex was first examined using surface stimulation by Woolsey and colleagues.[24,29,30] While numerous studies have been performed in the forelimb motor cortex, relatively few have focused on the hindlimb area, probably because of its relatively small size. Early studies reported purely bilateral representation of the hindlimb, in contrast to the contralateral representation of the forelimb. In more recent studies using intracortical microstimulation techniques, Hall and Lindholm reported that the rat hindlimb area has a predominantly contralateral representation and includes a complete overlap of the somatosensory and motor representations.[8]

Most ICMS studies of the motor cortex in the rat have been conducted in Sprague-Dawley,[8] Long-Evans,[2,17] or in unidentified strains of rat.[1,5] The stereotactic location of the hindlimb area in rat has been reported as close to Bregma as 0.0 mm posterior[17] or farther posterior, between 1.0 mm and 3.0 mm posterior to Bregma, and 1.5 mm and 3.5 mm lateral to Bregma (midline).[8] One study examining cortical organization of the motor area in different strains of rat showed that the size of the cortical movement representation was larger in Long-Evans rats compared to Fischer-344 rats and that a hindlimb area was not always identified in individual Fischer rats.[27]

The hindlimb movement representation seen here is similar to that reported by Neafsey et al. in Long-Evans rats, with hip movements found most medially and the knee, ankle and toe movements located more laterally.[17] The stereotactic location of the hindlimb area was more similar to that reported by Hall and Lindholm (1.5 mm to 3.5 mm posterior to Bregma)[8] than that observed by Neafsey et al., where the hindlimb area's rostral extent was reported to be at Bregma.[17] Minimum threshold current levels required to evoke hindlimb movements were similar to that reported in studies using similar ICMS parameters.[5,17]

The preponderance of contralaterally evoked hindlimb movements seen here is in agreement with those reported elsewhere, where bilateral responses are seen only at higher current

levels but not at threshold current levels.[8] This suggests that the completely bilateral representation of the hindlimb in early surface stimulation studies was due to the higher intensity of stimulation in those studies.[1,24,29,30]

With respect to the individual variation in hindlimb representations, the topographic details suggest that hindlimb maps are highly idiosyncratic. While the general location of the hindlimb area is reliable, there is considerable variability in the map details. It is not uncommon for some movements (knee, toe) not to be evoked in some animals. This is most likely a sampling issue. If the representation is particularly small (as is the hindlimb in general relative to the forelimb in other studies), higher resolution mapping might be needed, possibly beyond the resolution of the. However, the results reveal a remarkably consistent location across individual rats. A small cortical zone was found in all six rats where the hindlimb representation was found using minimum stimulation currents.

Advantages and limitations of ICMS studies of motor representations

ICMS has significant advantages for mapping details in motor representations since the microelectrode is advanced into layer 5, in the vicinity of the corticospinal neurons. Relatively low currents are required to evoke movements, even under ketamine anesthesia. This allows for high spatial resolution, on the order of 250 μm or less, or at least an order of magnitude greater than the resolution of non-invasive mapping techniques such as transcranial magnetic stimulation or even cortical surface stimulation. Thus, despite the small size of the rat hindlimb representation, it is possible to describe the internal topography in some detail.

However, it should be noted that movements evoked by ICMS may result from both direct excitation of local neurons and polysynaptic activation of more distant neurons. Since thresholds for movements were low (averaging 34 μA), the direct spread of current was limited to the immediate vicinity of the stimulating electrode and hence within the interpenetration distance of 250μm (see Stoney, Thompson and Asanuma; 1968).[25] However, more widespread polysynaptic effects from a wider area of cortex cannot be ruled out. Nevertheless, the relative stability of response at each site, and the often striking differences of each response between adjacent sites suggest that ICMS is a reliable technique for defining functional movement boundaries in motor cortex.[11,19]

The intent of the present study was to define the spatial distribution of the hindlimb representation across several animals to determine if the location, with respect to sterotactic coordinates, was predictable. The typical method of defining the movements evoked at near-threshold current levels was sufficient for this purpose. Thus, while the magnitude of movements (or alternatively, EMG potentials) might be informative for understanding additional details of motor map organization, it was not necessary for the intended purposes of this study.

Significance of present results for neuroprosthetic development

These findings are important since they may provide better rationale for the use of rodent models in the development of brain-computer-interfaces, especially for improving motor function after spinal cord injury. The need for methods to enhance neurologic recovery and function is well known, since there currently is no cure for spinal cord injury, and recent randomized clinical trials have been disappointing. Surgical decompression and sophisticated postoperative care are helpful in limiting secondary injury, and have allowed patients with spinal cord injury to live a virtually normal lifespan. Many patients are left with chronic paralysis, and thus, there is a need for some mechanism to restore function below the level of injury. Thoracic spinal cord injuries, for example, tend to produce

complete injures, and thus there may be limited feedback information from the spinal cord. Brain-computer-interfaces, in which control signals from the motor cortex are used to drive external devices, or stimulation of skeletal muscles, are becoming more feasible.[6,9] However, many challenging issues regarding the design parameters of such systems have yet to be overcome. The demonstration of reliability in the exact cortical localization of hindlimb (lower extremity) representations in rodent models may provide an experimental platform leading to the development of more precise ways of restoring neurologic function, and thus improving the quality of life, in patients harboring spinal cord injuries.

Clinical studies examining brain activity levels in the cortex of spinal cord-injured patients have reported activations in cortical areas involved in motor control (primary and secondary motor cortex) during attempts to move, or during mental imagery of movement tasks.[22] In the early subacute phase after spinal cord injury, injured patients had reduced activation within primary motor cortex and greater activation in secondary motor areas compared to controls.[12] In the later chronic phase, there is a progressive increase in M1 activation and decrease in secondary motor area activation in injured patients until activation is similar to that of controls.[12] In a review of brain activation studies of spinal cord injured patients, Kokotilo and colleagues reported that in many studies an increase in intensity of activation in cortical motor areas of spinal cord-injured patients above controls was observed, as well as activation of subcortical areas not active in controls.[14]

Based on these clinical studies, it appears that brain networks involved in motor control (both M1 and secondary areas) remain active and responsive, even in chronic paralysis.[14] This preserved brain activity that is linked to attempts to move, or to motor imagery can potentially be harnessed in therapeutic strategies for restoring motor function using brain-machine interfaces with the spinal cord below the level of injury.

To effectively use a rat model of spinal cord injury in the development of a brain-machine-spinal cord interface device, accessing the location of the hindlimb area is essential for utilizing intact activity. Identifying motor areas using standard ICMS procedures is not possible after severe spinal cord injury due to the damage to the descending cortical spinal tract. The findings reported here on the reliability of the hindlimb motor representation in rats with respect to stereotactic coordinates can be used to target the motor hindlimb area and utilize cortical activity that is preserved following spinal cord injury in the development of a potential therapeutic brain-machine interface device.

CONCLUSIONS

The location of the cortical hindlimb movement representation in Fischer-344 rats can be reliably located based on its stereotactic position relative to Bregma. The exact cortical localization of hindlimb representations may help lead to the development of more precise ways of restoring neurologic function after spinal cord injury through brain-computer interfaces.

Acknowledgments

This work was supported by a generous gift from the Ronald D. Deffenbaugh Foundation (Randolph J. Nudo) and NIH/NINDS R37 NS030853-20 (Randolph J. Nudo)

References

1. Angel A, Jolly AI, Lemon RN. A re-investigation of the sensorimotor cortical area for the hind leg in the rat. J Physiol. 1971; 215:18P–19P.

2. Barth TM, Jones TA, Schallert T. Functional subdivisions of the rat somatic sensorimotor cortex. Behav Brain Res. 1990; 39:73–95. [PubMed: 2390194]
3. Benton RL, Whittemore SR. VEGF165 therapy exacerbates secondary damage following spinal cord injury. Neurochem Res. 2003; 28:1693–1703. [PubMed: 14584823]
4. Cenci MA, Whishaw IQ, Schallert T. Animal models of neurological deficits: how relevant is the rat? Nat Rev Neurosci. 2002; 3:574–579. [PubMed: 12094213]
5. Donoghue JP, Wise SP. The motor cortex of the rat: cytoarchitecture and microstimulation mapping. J Comp Neurol. 1982; 212:76–88. [PubMed: 6294151]
6. Ethier C, Oby ER, Bauman MJ, Miller LE. Restoration of grasp following paralysis through brain-controlled stimulation of muscles. Nature. 2012; 485:368–371. [PubMed: 22522928]
7. Friel KM, Nudo RJ. Recovery of motor function after focal cortical injury in primates: compensatory movement patterns used during rehabilitative training. Somatosens Mot Res. 1998; 15:173–189. [PubMed: 9874517]
8. Hall RD, Lindholm EP. Organization of motor and somatosensory neocortex in the albino rat. Brain Research. 1974; 66:23–38.
9. Hochberg LR, Bacher D, Jarosiewicz B, Masse NY, Simeral JD, Vogel J, et al. Reach and grasp by people with tetraplegia using a neurally controlled robotic arm. Nature. 2012; 485:372–375. [PubMed: 22596161]
10. Hollis ER 2nd, Lu P, Blesch A, Tuszynski MH. IGF-I gene delivery promotes corticospinal neuronal survival but not regeneration after adult CNS injury. Exp Neurol. 2009; 215:53–59. [PubMed: 18938163]
11. Huang CS, Sirisko MA, Hiraba H, Murray GM, Sessle BJ. Organization of the primate face motor cortex as revealed by intracortical microstimulation and electrophysiological identification of afferent inputs and corticobulbar projections. J Neurophysiol. 1988; 59:796–818. [PubMed: 2835448]
12. Jurkiewicz MT, Mikulis DJ, McIlroy WE, Fehlings MG, Verrier MC. Sensorimotor cortical plasticity during recovery following spinal cord injury: a longitudinal fMRI study. Neurorehabil Neural Repair. 2007; 21:527–528. [PubMed: 17507643]
13. Kleim JA, Barbay S, Nudo RJ. Functional reorganization of the rat motor cortex following motor skill learning. J Neurophysiol. 1998; 80:3321–3325. [PubMed: 9862925]
14. Kokotilo KJ, Eng JJ, Curt A. Reorganization and preservation of motor control of the brain in spinal cord injury: a systematic review. J Neurotrauma. 2009; 26:2113–2126. [PubMed: 19604097]
15. Loy DN, Crawford CH, Darnall JB, Burke DA, Onifer SM, Whittemore SR. Temporal progression of angiogenesis and basal lamina deposition after contusive spinal cord injury in the adult rat. J Comp Neurol. 2002; 445:308–324. [PubMed: 11920709]
16. Master D, Cowan T, Narayan S, Kirsch R, Hoyen H. Involuntary, electrically excitable nerve transfer for denervation: results from an animal model. J Hand Surg Am. 2009; 34:479–487. 487 e471–473. [PubMed: 19258146]
17. Neafsey EJ, Bold EL, Haas G, Hurley-Gius KM, Quirk G, Sievert CF, et al. The organization of the rat motor cortex: a microstimulation mapping study. Brain Res. 1986; 396:77–96. [PubMed: 3708387]
18. Nudo, RJ.; Frost, SB. The evolution of motor cortex and motor systems, Chapter 14. In: Krubitzer, LH.; Kaas, JH., editors. Evolution of Nervous Systems: A Comparative Reference, Volume 4 – Evolution of Nervous System in Mammals. Oxford, UK: Elsevier; 2006.
19. Nudo RJ, Jenkins WM, Merzenich MM, Prejean T, Grenda R. Neurophysiological correlates of hand preference in primary motor cortex of adult squirrel monkeys. J Neurosci. 1992; 12:2918–2947. [PubMed: 1494940]
20. Nudo RJ, Masterton RB. Descending pathways to the spinal cord: a comparative study of 22 mammals. J Comp Neurol. 1988; 277:53–79. [PubMed: 3198796]
21. Nudo RJ, Milliken GW, Jenkins WM, Merzenich MM. Use-dependent alterations of movement representations in primary motor cortex of adult squirrel monkeys. J Neurosci. 1996; 16:785–807. [PubMed: 8551360]

22. Sabbah P, de Shonen S, Leveque C, Gay S, Pfefer F, Nioche C. Sensorimotor cortical activity in patients with complete spinal cord injury: a functional magnetic resonance imaging study. J Neurotrauma. 2002; 19:53–60. [PubMed: 11852978]

23. Sandner B, Pillai DR, Heidemann RM, Schuierer G, Mueller MF, Bogdahn U, et al. In vivo high-resolution imaging of the injured rat spinal cord using a 3.0T clinical MR scanner. J Magn Reson Imaging. 2009; 29:725–730. [PubMed: 19243068]

24. Settlage PH, Binghan WG, Suckle HM, Borge AF, Woolsey CN. The pattern of localization in the motor cortex of the rat. Fed Proc. 1949; 8:144.

25. Stoney SD Jr, Thompson WD, Asanuma H. Excitation of pyramidal tract cells by intracortical microstimulation: effective extent of stimulating current. J Neurophysiol. 1968; 31:659–669. [PubMed: 5711137]

26. Tyler BM, Hdeib A, Caplan J, Legnani FG, Fowers KD, Brem H, et al. Delayed onset of paresis in rats with experimental intramedullary spinal cord gliosarcoma following intratumoral administration of the paclitaxel delivery system OncoGel. J Neurosurg Spine. 2012; 16:93–101. [PubMed: 22208429]

27. VandenBerg PM, Hogg TM, Kleim JA, Wishaw IQ. Long-Evans rats have a larger cortical topographic representation of movement than Fischer-344 rats: a microstimulation study of motor cortex in naive and skilled reaching-trained rats. Brain Res Bull. 2002; 59:197–203. [PubMed: 12431749]

28. Weber T, Vroemen M, Behr V, Neuberger T, Jakob P, Haase A, et al. In vivo high-resolution MR imaging of neuropathologic changes in the injured rat spinal cord. AJNR Am J Neuroradiol. 2006; 27:598–604. [PubMed: 16552001]

29. Woolsey, CN. Biology Of Mental Health and Disease. New York: Hoeber; 1952. Patterns of localization in sensory and motor areas of the cerebral cortex; p. 193-206.

30. Woolsey, CN. Organization of somatic sensory and motor areas of the cerebral cortex. In: Harlow, HF.; Woolsey, CN., editors. Biological and Biochemical Bases of Behavior. Madison: University of Wisconsin Press; 1958. p. 63-81.

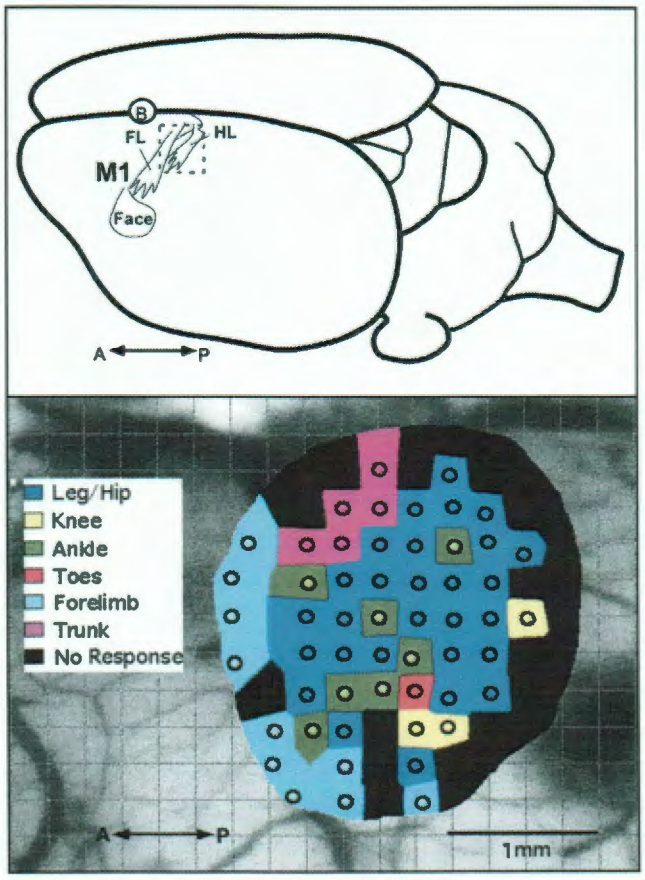

FIG. 1.

Top: Schematic diagram of a dorsolateral view of the rat brain showing the location of the hindlimb representation (HL) relative to the forelimb (FL) and face representations in primary motor cortex (M1) of the left hemisphere. The circled B indicates the position of Bregma on the dorsal surface of the skull at midline over the longitudinal convexity. Bottom: Results of ICMS mapping of the hindlimb representation in the left hemisphere in a representative F344 rat (R33). Circles represent the location of microelectrode penetrations and colors represent the movement evoked by near-threshold electrical stimulation (<70 μA). In this rat the total hindlimb area measures 2.51 mm^2. A = anterior; P = posterior.

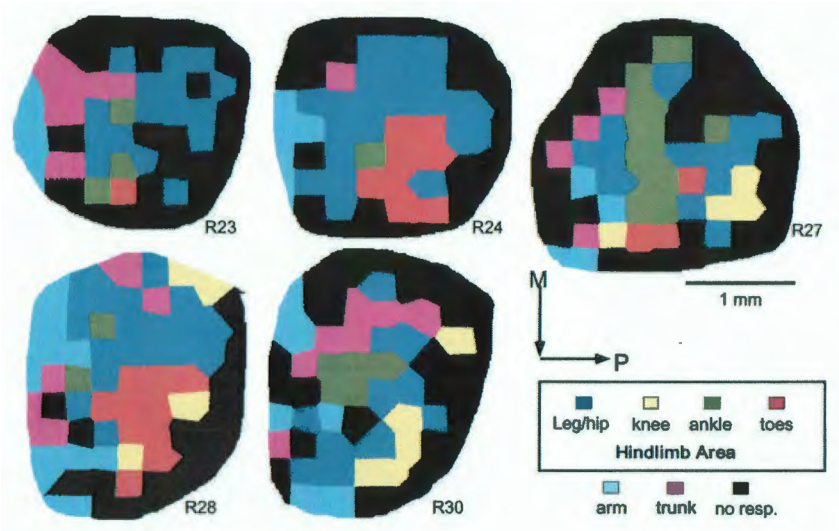

FIG. 2.

Results of ICMS mapping experiments in the remaining 5 rats. Area measurements of hindlimb movement representations are listed in Table 1. M= medial; P= posterior. 1mm scale bar is for all maps.

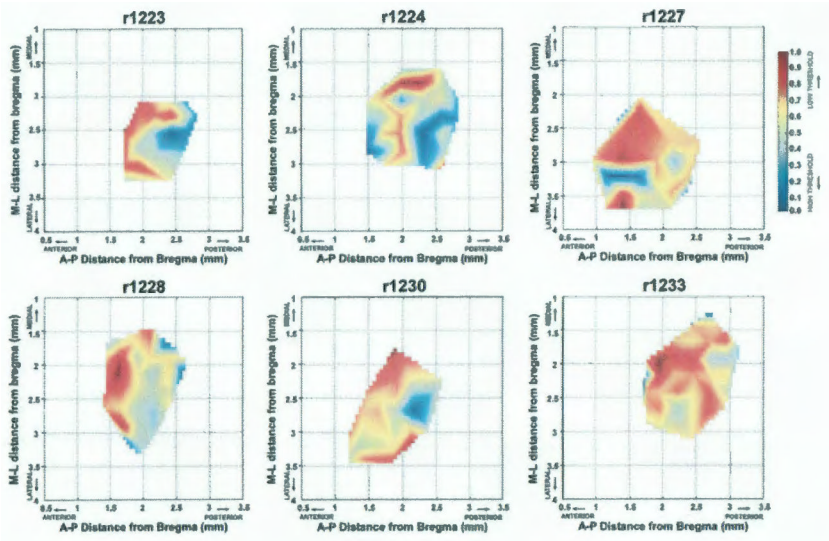

FIG. 3.

Graphical distribution of minimum currents required to evoke hindlimb movements (movement thresholds) in each of the six rats. Current values for each map were normalized across the range of currents from minimum to maximum, such that minimum (lowest) thresholds = 1 and appear in red and the maximum (highest) thresholds = 0 and appear in blue. A MatLAB® algorithm was used to interpolate values to create a continuous distribution. M= medial; L= lateral; A= anterior; P= posterior

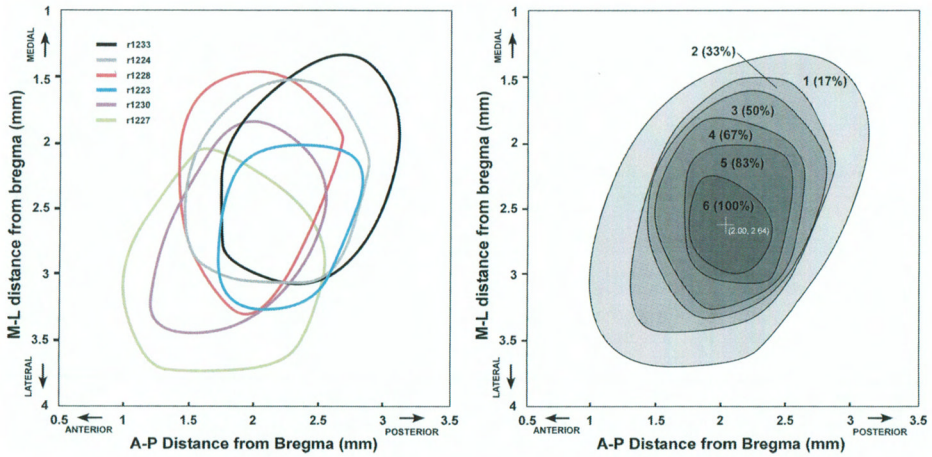

FIG. 4.

Left: Overlay of hindlimb representation borders relative to Bregma for each rat. Borders are derived from movement maps illustrated in Figure 1–2, and are created by a smoothing algorithm based on locations of individual boundary sites (Canvas, ACD Systems). Right: Hindlimb probability map showing the degree of overlap of hindlimb representations in the sample of six rats. Greyscale and numbers indicate the number of rats with hindlimb representation at a particular stereotactic location. The darkest region (6) represents the territory in which hindlimb movements are evoked in all six rats (100%). The center of the overlap region is located at 2.00 mm posterior and 2.64 mm lateral to Bregma. M= medial; L= lateral; A= anterior; P= posterior.

Table 1

Area Measurements (mm^2) of Hindlimb Movement Representations

Rat#	Leg/Hip	Knee	Ankle	Toes	Total HL
R23	0.98	0	0.19	0.06	1.23
R24	1.58	0	0.07	0.60	2.25
R27	0.90	0.26	0.75	0.19	2.10
R28	1.28	0.28	0.12	0.68	2.36
R30	0.87	0.37	0.32	0	1.56
R33	1.81	0.18	0.47	0.05	2.51
X+/− SE	1.24+/− 0.39	0.18+/− 0.15	0.32+/− 0.26	0.26+/− 0.30	2.00+/− 0.50

Table 2

Minimum Hindlimb Movement Thresholds (μA)

Rat#	Leg/Hip	Knee	Ankle	Toes	Forelimb	Total HL
R23	41.2+/− 15.3	NA	35.3+/− 13.6	25.0	35.0+/− 14.7	40.3+/− 14.9
R24	38.5+/− 12.7	NA	25.0	40.6+/− 14.9	35.7+/− 12.6	38.5+/− 13.1
R27	35.8+/− 10.0	38.3+/− 18.8	33.9+/− 14.6	28.7+/− 11.5	35.0+/− 3.7	34.7+/− 12.3
R28	29.1+/− 14.6	40.0+/− 10.0	17.7+/− 4.5	35.9+/− 6.0	30.6+/− 12.9	31.3+/− 12.6
R30	31.6+/− 13.0	22.3+/− 10.4	26.0+/− 2.0	NA	46.0+/− 16.4	28.4+/− 11.1
R33	29.3+/− 11.8	35.3+/− 21.2	28.7+/− 7.1	30.0	32.2+/− 20.3	29.7+/− 11.4
Avg. X+/− SD	34.3+/− 5.0	34.0+/− 8.0	27.8+/− 6.4	32.0+/− 6.2	35.7+/− 5.4	33.8+/− 4.8